JGR Space Physics

RESEARCH ARTICLE
10.1029/2019JA027359

Active (Evolving) Phase of Equatorial Plasma Bubbles Observed Over Tirunelveli

B. Kakad[1], P. Gurram[1], A. Bhattacharyya[2], and D. S. V. V. D. Prasad[3]

[1]Indian Institute of Geomagnetism, Navi Mumbai, India, [2]CSRE, Indian Institute of Technology, Mumbai, India, [3]Department of Physics, Andhra University, Visakhapatnam, India

Key Points:
- On disturbed days, FESF with longer active phase are more likely during low solar flux
- Quiet time weaker westward ambient electric field assists in survival of perturbation electric field of FESF for longer time
- FESF generated on days with stronger magnetic activity tend to have longer active phase

Correspondence to:
B. Kakad,
bkakad9@gmail.com

Citation:
Kakad, B., Gurram, P., Bhattacharyya, A., & Prasad, D. S. V. V. D. (2020). Active (evolving) phase of equatorial plasma bubbles observed over Tirunelveli. *Journal of Geophysical Research: Space Physics*, *125*, e2019JA027359. https://doi.org/10.1029/2019JA027359

Received 5 SEP 2019
Accepted 19 AUG 2020
Accepted article online 22 AUG 2020

Abstract Usual post-sunset generation of equatorial spread F (ESF) irregularities on quiet days (Q-days) and midnight or post-midnight generation of ESF on magnetically disturbed days (D-days) is widely known. However, the duration of evolving or active phase of these freshly generated ESF (FESF) irregularities is not clearly understood. Here, the active phase duration refers to the time period during which the perturbation electric field associated with equatorial plasma bubbles drifting over Tirunelveli is alive. Recently, Gurram et al. (2018) quantified the active phase duration of FESF for both Q-days and D-days. It was the first exercise to obtain the average active phase duration of FESF from observations. In view of this, we carried out detailed analysis to examine their dependence on solar flux and geomagnetic activity using long-term amplitude scintillation observations on 251-MHz signal. It is found that percentage of days with longer active phase ($t_d \geq 50$ min) is higher on D-days, and it is consistent for all levels of solar flux. Average duration of the active phase of FESF, $\langle t_d \rangle$, is 57.9 ± 52.3 min on D-days and 33.8 ± 23.4 min on Q-days. The active phase of FESF has tendency to sustain for longer time during low solar flux, which is attributed to presence of weaker ambient ionospheric electric field during that period. It is noted that FESF generated on days with stronger geomagnetic activity tend to have longer active phase. Also, days with FESF cause more moderate–strong scintillations as compared to days with drifted-in ESF.

1. Introduction

We know that the equatorial plasma bubbles (EPBs) are formed in the post-sunset hours through growth of the generalized Rayleigh-Taylor (GRT) instability in the close vicinity of magnetic equator, where magnetic field is nearly horizontal. The nonlinear evolution of this plasma instability leads to the generation of electron density irregularities, commonly known as equatorial spread F (ESF) irregularities, which vary from few centimeters to hundreds of kilometers. Various ambient ionospheric conditions like strength of pre-reversal enhancement (PRE) of the eastward electric field, vertical density gradient at the bottom side of *F* region, ion-neutral collisions, horizontal conductivities in E region, alignment of sunset terminator and magnetic meridian, neutral winds, and strength of ambient magnetic field play an important role in deciding the genesis of EPBs (Abdu et al., 2008; Basu et al., 1996; Bhattacharyya, 2004; Patra et al., 1997; Tsunoda, 1985). Worldwide efforts have led to a situation where we have gathered fairly good understanding about EPBs through theory, observations, and simulations (Bhattacharyya et al., 2019; Burke et al., 2004; Carter et al., 2014; Engavale & Bhattacharyya, 2005; Fejer, 1997; Navarro et al., 2019; Ossakow, 1981; Retterer, 2010; Sultan, 1996; Yokoyama et al., 2014). But day-to-day generation of scintillation producing irregularities in the low-latitude ionosphere is still a challenging question from the prediction point of view. A seed perturbation of appropriate scale and strength is required for the initiation of GRT plasma instability in the post-sunset hours (Sekar et al., 1995). Generally, gravity waves, spatially varying electric field, and large-scale wave structures are the common sources for such seed perturbation (Huang & Kelley, 1996a, 1996b; Hysell et al., 1990; Joshi et al., 2015; Krall et al., 2013; Narayanan et al., 2012; Patra et al., 2013; Tsunoda, 2012). In recent simulations, it is shown that vertical wind of amplitude as low as 5 m/s can seed EPBs effectively (Yokoyama et al., 2019). Some data-based models are also available for the prediction of ESF, and these models can be improved by adding more data from global perspective (Abdu, Souza, et al., 2003; Bilitza et al., 2017). Apart from occurrence of EPBs, their structuring is also important because the strength and spatial structures of the ESF irregularities decide the degradation caused to radio signals (e.g., very-high frequency, ultra-high frequency and L-band) that are passing through such irregular medium (Kakad et al., 2016; Keskinen et al., 2006). The occurrence of L-band scintillation in the

anomaly region (where the ambient plasma density is higher) is mainly controlled by the presence/absence of ESF irregularities with shallower power spectrum (smaller spatial scales) in that region (Bhattacharyya et al., 2017). In recent study, occurrence of ESF irregularities generated as a result of magnetic activity has been studied statistically, and it is reported that during the active phase of evolution, these FESF irregularities cause more moderate–strong scintillations on very high frequency (VHF) radio signal as compared to the quiet time (Gurram et al., 2018).

Another important issue is that we do not have much information about the duration of active phase of EPBs. The active phase of EPBs is linked to the nonlinear evolution of GRT plasma instability. If we want information about the duration of perturbation electric field associated with GRT plasma instability, then one has to track the same EPB from the time of its initiation until the time of decay of this perturbation electric field. But with presently available observational techniques tracking of the same EPB for a long time is not possible because EPBs drift upward and eastward after their generation. In the present study, the active phase duration refers to the time duration for which the perturbation electric field associated with EPBs drifting over Tirunelveli is alive (not eroded significantly). It may be noted that we need some proxy parameter in order to confirm the survival of perturbation electric field associated with the EPBs drifting overhead. In this context, Bhattacharyya et al. (1989) observed that the random velocities estimated from spaced receiver scintillations are higher in the initial phase (<22 LT) of a magnetically quiet time equatorial scintillation event in the post-sunset hours. The random velocity is a measure of random changes in the ESF irregularity characteristics, and their higher values are attributed to the random velocity fluctuations caused by the perturbation electric field associated with GRT plasma instability responsible for generation of the ESF irregularities. In general, for quiet days (Q-days), it has been noticed that the perturbation electric field dies down approximately within 2 h after their generation in the post-sunset hours (Bhattacharyya et al., 1989, 2001). Although this perturbation electric field gets eroded within few hours, the generated density structures can remain and drift with ambient plasma to cause amplitude or phase scintillations through the night. On a day-to-day basis, the nature of the perturbation electric field can be different depending on the nonlinear evolution of the EPBs. We do not have much information about the duration of the perturbation electric field of EPBs. Recently, Gurram et al. (2018) for the first time estimated the average duration of active phase of EPBs drifting over Tirunelveli using long-term VHF scintillation observations. In their study, efforts have been made to quantify the active phase duration, and it is reported that the perturbation electric field linked with the FESF survives for more time on magnetically disturbed days (D-days) as compared to that on Q-days. However, dependence of the active phase duration of the FESF on the solar flux and strength of geomagnetic activity have not been quantified so far. To examine this dependence, we have carried out detailed analysis in the present paper.

The paper is organized as follows. The data used and analysis technique are briefly discussed in section 2. The estimation of active phase duration of FESF is discussed in section 3. Results are explained in section 4. The observed tendencies are discussed in light of possible physical mechanisms in section 5. The present work is summarized and concluded in section 6.

2. Data Used and Analysis Technique

We have utilized amplitude scintillation data for a 251-MHz signal transmitted from a geostationary satellite and recorded by two spaced receivers aligned in the magnetic east–west direction at the dip equatorial station Tirunelveli (8.7°N, 77.8°E) during 1992–2006 and 2013–2015. The dip angle at observation station varied between 0.7° to 2.9° during this period. The signal was transmitted from geostationary satellite FLEETSAT (73°E) during 1992–2000, UFO2 (71.3°E) during 2000–2006, and UFO10 (72.4°E) during 2013–2015. The sampling intervals of scintillation data are 0.1 s before 2013 and 0.05 s after 2013. Spaced receivers are separated by a distance of 540 m. It may be noted that although we have used scintillation observations during 1992–2006 and 2013–2015 (total 216 months), the experiment was not running continuously during this period. For example, during 1992, it was functioning only for 2 months (September and October). Altogether, the scintillation experiment was functioning for 92 months. The details of these months and corresponding number of days with scintillations are shown in Figure 1. There are total 1,403 days of scintillation observation, which has 1,006 Q-days and 397 D-days. On majority of days (1,373 days), scintillations are observed during 18–30 LT, whereas it occasionally (30 days, 2%) extends beyond 30 LT up to 34 LT. Here, 30–34 LT represents 06–10 LT of the following day. In addition, we used 10.7-cm solar flux data (1-day resolution) from NGDC NOAA, interplanetary magnetic field (IMF) data (5-min resolution), *SYMH* (5-min resolution)

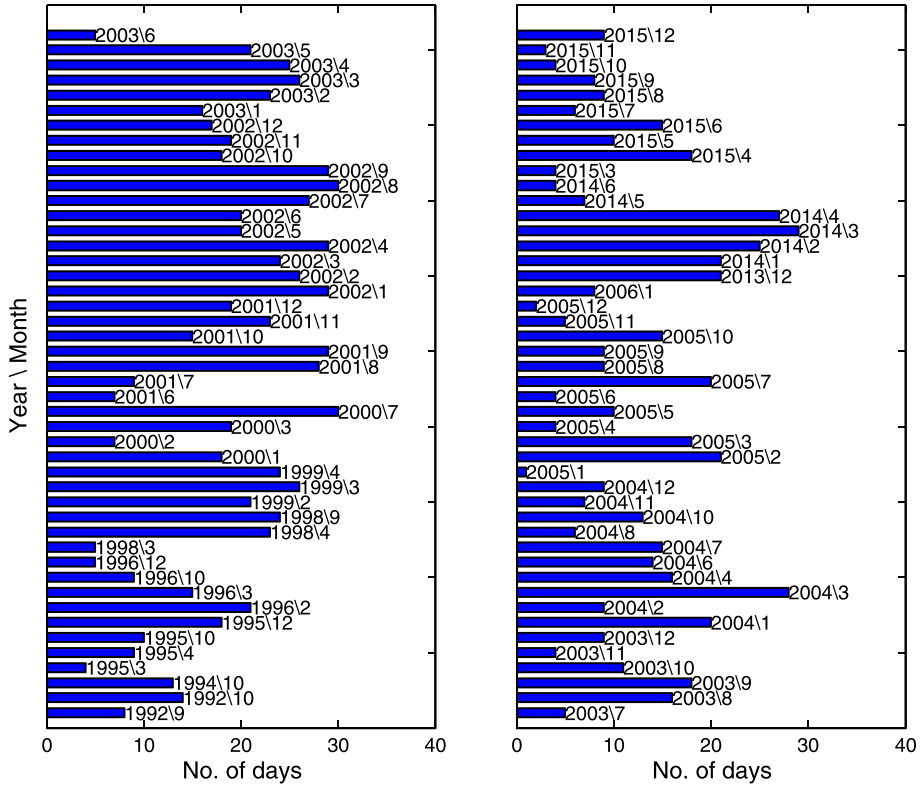

Figure 1. Months for which scintillation data were available during the periods of 1992–2006 and 2013–2015.

from CDAWEB, and geomagnetic activity indices like *Kp* (3-h resolution) from WDC Kyoto. We separated the days into quiet and disturbed category based on the midlatitude geomagnetic activity index, *Kp*. We have used interplanetary solar wind velocity and magnetic field to compute interplanetary electric field (IEF; i.e., $\vec{E} = -\vec{V} \times \vec{B}$). The $+y$ component of electric field represents the dawn–dusk IEF, which is $E_y = V_x B_z - V_z B_x$.

Spaced receiver scintillation technique can be used to get the information about average drift speed of ESF irregularity (Bhattacharyya et al., 1989; Ledvina et al., 2004; Valladares et al., 1996) and the dominant spatial scale associated with the ground scintillation pattern (Bhattacharyya et al., 2003; Engavale et al., 2005; Gurram et al., 2019). The ESF irregularities follow a power law spectrum, and the intermediate-scale irregularities (100 m to 10 km) contribute to amplitude scintillations on VHF signals. We used the full cross-correlation technique (Briggs, 1984) to analyze the spaced receiver amplitude scintillation data. Here, the space-time correlation function is assumed to have the following form:

$$C_I(x,t) = f[(x - V_0 t)^2 + V_c^2 t^2], \tag{1}$$

where f is a monotonically decreasing function of its argument and it has maximum at zero, that is, $f(0) = 1$. This technique is elaborated in Bhattacharyya et al. (1989). We basically estimate S_4, $C_I(x_0,t_m)$, V_0, and V_c for every 3-min interval using the spaced receiver measurements of amplitude scintillations. S_4 index, which is the standard deviation of normalized intensity fluctuations, is a measure of strength of scintillation. The average drift speed of scintillation pattern along the receivers' baseline is V_0, and V_c is the random velocity, a measure of random changes in the irregularity characteristics. The maximum cross-correlation between intensity variations recorded by two receivers is given by $C_I(x_0,t_m)$, which has occurred at a time lag of t_m. The drift speed of irregularities across the signal path affects the lag t_m, whereas the changes in characteristic of these irregularities affect $C_I(x_0,t_m)$. The parameter $C_I(x_0,t_m)$ is important as it is used to identify the FESF irregularities, which is elaborated in the next section.

3. Estimation Active Phase Duration of FESF

In the present study, identification of FESF is an important task as we are investigating the active phase duration of ESF irregularities. The amplitude or phase scintillations observed at a given location may be

caused by the EPBs generated overhead at that location or the EPBs drifted in from a distant west-side location of the observation station. By considering this aspect, Bhattacharyya et al. (2002) identified the EPBs generated freshly as a result of magnetic activity. These authors used random velocity, V_c, to identify the freshly generated EPBs. As discussed in the previous section, V_c is a measure of random changes in the irregularity characteristics and it is directly related to $C_I(x_0, t_m)$: V_c increases as $C_I(x_0, t_m)$ decreases. However, V_C cannot be estimated when $C_I(x_0, t_m) < 0.5$, whereas a decrease in $C_I(x_0, t_m)$ does indicate greater random changes. Thus, one can use maximum of space-time cross-correlation function, $C_I(x_0, t_m)$, which is estimated throughout a scintillation event, to get information about the FESF intervals. $C_I(x_0, t_m)$ is a statistical parameter varying between 0 and 1. This technique is in general valid for all LT, Q-days and D-days, seasons, and solar flux conditions. Subsequently, by adopting this method, different studies were carried out to address local time, season, solar flux, and magnetic activity dependence of the FESF irregularities and their spatial structures and power spectral characteristics (Bhattacharyya et al., 2003; Engavale et al., 2005; Gurram et al., 2018; Kakad et al., 2007, 2012a). Using simultaneous radar and scintillation observations, it is shown that the spectral width estimated from the radar can be used to identify the freshly generated EPBs (Tiwari et al., 2006). Apart from this, Ajith et al. (2016) attempted to categorize evolving type and drifted-in type EPBs based on the visual inspection of fan sector map of equatorial atmospheric radar located at Kototabang, Indonesia. However, these authors have not used any proxy parameters to identify and confirm the evolving or drifted-in EPBs. Recently, based on radar echo spectral width, Joshi et al. (2019) suggested that the drifted-in EPBs are less evolving type. In the present case, the signal is transmitted from geostationary satellite. The zenith and azimuth angles for the signal were 11.4°, 209°; 12.8°, 216.9°; and 12.8°, 216.9° during 1992–2000, 2000–2006, and 2013–2015, respectively. For this period, the latitude and longitude of ionospheric penetration point (IPP) for signal crossing the ionosphere at 300 km come out to be ≈8.3° and 77.5°, which is almost overhead to the observation station Tirunelveli (lat. 8.7°, long. 77.8°). Thus, we confirm that the observed scintillations are caused by the ESF irregularity drifting overhead. Now, these overhead irregularities can be either FESF or drifted-in ESF and we can identify them based on $C_I(x_0, t_m)$.

We record scintillations at a fixed location with two spaced receivers. We cannot pinpoint the exact location of the generation of EPBs. In the post-sunset hours, after their generation, the EPBs generally drift upward and eastward, while structures or irregularities develop within them. When the EPBs drift over Tirunelveli, the intermediate-scale irregularities contribute to the scintillations observed at that particular time. We are tracking whatever is overhead at different times, and if the overhead ESF irregularities are able to cause high decorrelation (i.e., lower values of $C_I(x_0, t_m)$) between intensity variations recorded by two spaced receivers on ground, then it is an indication that the perturbation electric field associated with the overhead ESF is alive. As long as the perturbation electric field associated with the overhead ESF is sufficiently strong to cause low $C_I(x_0, t_m)$, it will be treated as FESF. These FESF irregularities are mostly drifting eastward in the post-sunset hours with average speed, $\langle V_0 \rangle = 131 \pm 30$ m/s. The EPBs are highly structured with spatial scales ranging from few hundred kilometers down to submeter. Such large-scale structure itself will take few tens of minutes to drift across the observation station. In such scenario, mostly the EPBs generated in the close neighborhood (within 1–1.5° westward) of Tirunelveli will get considered under FESF category.

We have used the maximum cross correlation between intensity variations recorded by two spaced receivers to pick the scintillation intervals that are linked with the FESF irregularities. As mentioned earlier, for each day, scintillation periods with $C_I(x_0, t_m) \leq 0.7$ are considered as the intervals of FESF. It may be noted that we have estimated $C_I(x_0, t_m)$ for every 3 min and our sampling is 10 Hz (or 20 Hz). It means that in our full cross-correlation technique, we take nearly 1,800 (or 3,600) amplitude scintillation samples to compute correlation functions. We know that ESF irregularity roughly drifts with speed of 50–200 m/s; hence, there will be quite a few ESF density structures moving overhead of spaced receivers in 3 min, and they will manifest their signatures in the ground scintillation pattern. Hence, smaller values of $C_I(x_0, t_m)$ imply that the characteristics of ESF irregularities producing these amplitude scintillations have been changed considerably in this 3-min interval. In Figure 2, we have illustrated two examples of Q-days (upper panels) and two examples of the D-day (lower panels), where FESF signatures are manifested in the ground scintillation pattern. From Figures 2a (13 October 2002; $\Sigma kp = 11$) and 2b (2 September 2003; $\Sigma kp = 20$), it is noted that $C_I(x_0, t_m)$ is low in the initial phase, which is attributed to the perturbation electric field associated with the GRT plasma instability responsible for the generation of ESF irregularities (Bhattacharyya et al., 2001). But in the later phase (>22 LT), this perturbation electric field gets eroded considerably, resulting in less change in the characteristics of the ESF irregularities, and hence, the signals from two receivers are well correlated. Here,

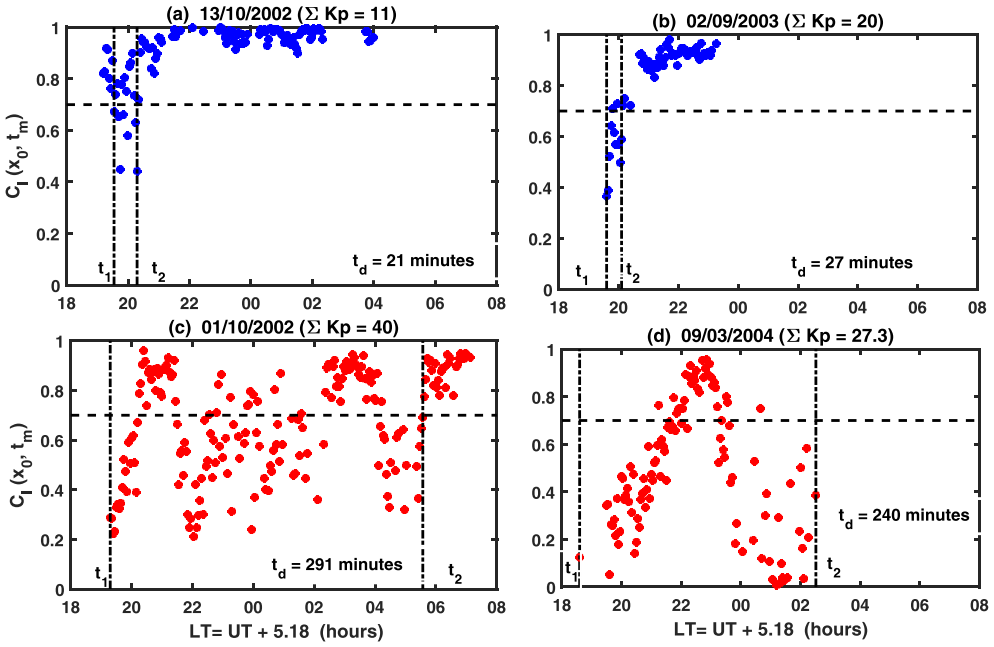

Figure 2. Variation of maximum cross correlation between intensity variations recorded by two spaced receivers, that is, $C_I(x_0, t_m)$ as a function of local time (LT = UT + 5.18) is shown for two Q-days, namely, (a) 13 October 2002 ($\Sigma Kp = 11$) and (b) 2 September 2003 ($\Sigma Kp = 20$), and two D-days, (c) 1 October 2002 ($\Sigma Kp = 40$) and (d) 9 March 2004 ($\Sigma Kp = 27.3$). The time intervals having $C_I(x_0, t_m) \leq 0.7$ are used to identify the FESF irregularities. The horizontal dotted line represents the $C_I(x_0, t_m) = 0.7$. The vertical dashed-dotted lines indicate the first (t_1) and the last (t_2) time instance that are associated with $C_I(x_0, t_m) = 0.7$ on a given night. The values of active phase durations t_d are given in respective subplots.

$C_I(x_0, t_m) = 1$ indicates perfect correlation of the two signals with a time lag of t_m determined by the spatial separation x_0 of the receivers and a constant drift speed of the irregularities across the signal path, during the 3-min interval for which the correlation is computed. Here, we have used the limit of 0.7 on $C_I(x_0, t_m)$. It may be noted that when $C_I(x_0, t_m) > 0.7$, the perturbation electric field associated with EPBs is not completely zero, but it is eroded significantly so that it is not affecting irregularity characteristics significantly.

Unlike Q-days, on magnetically D-days, the lower values of $C_I(x_0, t_m)$ are seen even after 22 LT, which indicates the fresh generation of EPBs at other times as well. Two such examples are shown in Figures 2c (1 October 2002; $\Sigma kp = 40$) and 2d (9 March 2004; $\Sigma kp = 27.3$). For each day, we estimated the active phase duration of FESF in minutes as $t_d = 3 \times N$ where N is the number of 3-min intervals that are having $C_I(x_0, t_m) \leq 0.7$. In the present analysis, the lower limit of $N = 3$ is applied to confirm the presence of perturbation electric field continuously for a minimum time interval of 9 min. It ensures the selection of genuine FESF intervals. The active phase duration of FESF is given in respective subplots for the examples shown in Figure 2. The horizontal dotted line shown in Figure 2 represents $C_I(x_0, t_m) = 0.7$, whereas vertical dash-dotted lines indicate the first time (t_1) and the last time (t_2) instance, where $C_I(x_0, t_m) \leq 0.7$ for a given day. It means that before time t_1 and after time t_2, no FESF is seen on a given day. Here, t_1 and t_2 provide information about the local times contributing to the active phase duration of FESF. It may be noted that for a given day, t_d gives the active phase duration of FESF that has occurred between time t_1 and t_2. But this FESF active phase may or may not be continuous as shown in Figures 2c and 2d. Thus, the FESF active phase duration estimated here may be sometimes associated with one or more freshly generated EPBs during the night. This way, we compiled t_d, t_1, and t_2 for all 525 days of scintillations that are caused by FESF irregularities.

As mentioned earlier, we have total 1,403 days of scintillation observations. These observed scintillations may be linked with either FESF or drifted-in ESF irregularities. Higher values of $C_I(x_0, t_m)$ indicate that signals from two spaced receivers are in good correlation and it is a signature of considerable weakening of perturbation electric field associated with EPBs. Four examples of drifted-in ESF observed at Tirunelveli are shown in Figure 3. Upper panels (Figure 3a, 17 January 2003, $\Sigma kp = 13.6$; Figure 3b, 29 June 2001,

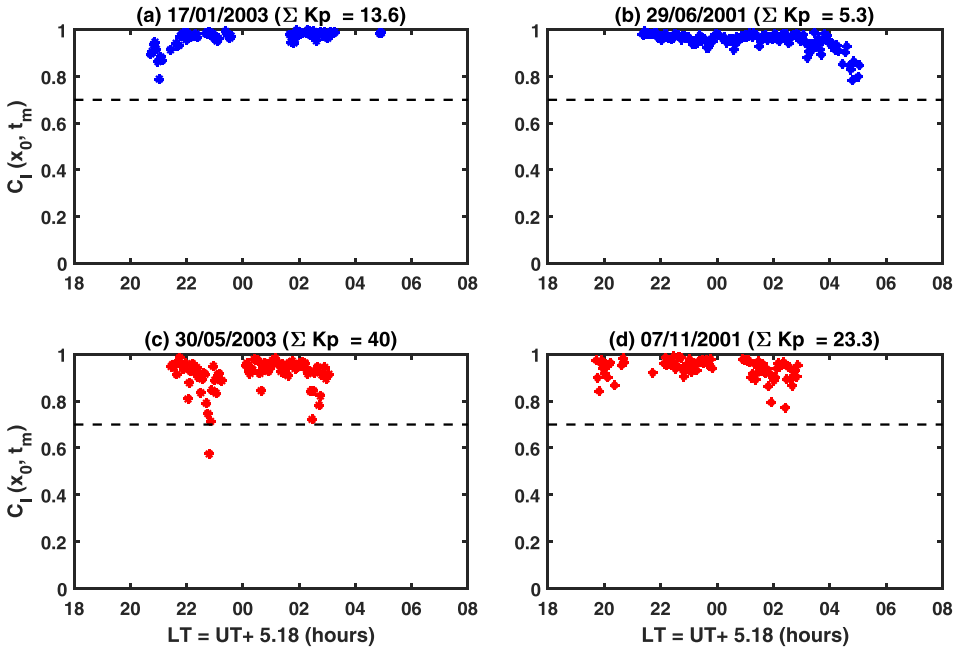

Figure 3. Variation of maximum cross correlation between intensity variations recorded by two spaced receivers, that is, $C_I(x_0, t_m)$, as a function of local time (LT = UT + 5.18) is shown for two Q-days, namely, (a) 17 January 2003 ($\Sigma Kp = 13.6$) and (b) 29 June 2001 ($\Sigma Kp = 5.3$), and two D-days, (c) 30 May 2003 ($\Sigma Kp = 40$) and (d) 7 November 2011 ($\Sigma Kp = 23.3$). These days are considered under drifted-in type EPBs as $C_I(x_0, t_m) > 0.7$ implies considerable weakening of the associated perturbation electric field. The horizontal dashed line represents $C_I(x_0, t_m) = 0.7$.

$\Sigma kp = 5.3$) and lower panels (Figure 3c, 30 May 2003, $\Sigma kp = 40$; Figure 3d, 7 November 2001, $\Sigma kp = 23.3$) are for two Q-days and two D-days, respectively. On these days, $C_I(x_0, t_m)$ has not sustained below 0.7 for minimum of 9 min or more. It suggests that the ESF irregularities causing these scintillations are not changing significantly any longer. Hence, such cases can be considered as days with drifted-in ESF. We have total 525 days with FESF and remaining days are drifted-type ESF as observed at Tirunelveli. The average start time of scintillation ($S_4 \geq 0.15$) for fresh and drifted-in type ESF irregularities are 19.9 ± 1.3 and 22 ± 2.5, respectively. We have checked the distribution of S_4 for days with drifted-in ESF and FESF for three different levels of scintillations, namely, weak ($0.15 \leq S_4 < 0.5$), moderate ($0.5 \leq S_4 < 1$), and strong ($S_4 \geq 1$). The occurrence distribution of S_4 is shown in Figure 4. The S_4 index is the measure of strength of scintillation, and it is controlled by the irregularity spatial scales and its strength. We noticed that the occurrence of moderate–strong scintillations is more prevalent on days with FESF as compared to days with drifted-in ESF. Another noticeable feature is that 878 days of drifted-in ESF produce 21,875 scintillations of 3-min interval, whereas 525 days of FESF give rise to 49,492 scintillations of 3-min interval. It is because scintillations are generally delayed for the days with drifted-type ESF, resulting in smaller scintillation duration on a given night.

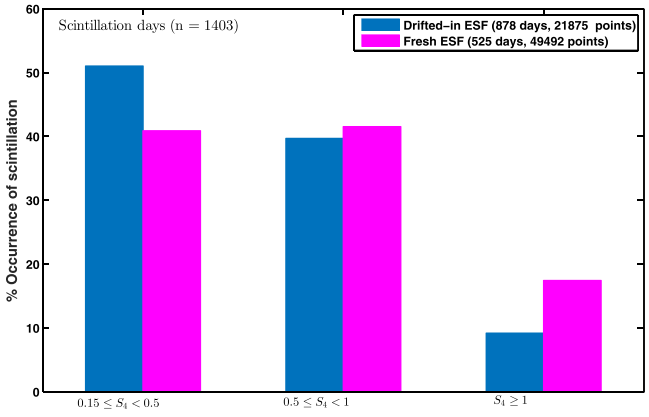

Figure 4. The percentage occurrence of scintillations in three different bins of S_4, namely, weak ($0.15 \leq S_4 < 0.5$), moderate ($0.5 \leq S_4 < 1$), and strong ($S_4 \geq 1$), for days with FESF (525 days) and drifted-in ESF (878 days).

4. Results

As our main interest is to understand the active phase of FESF observed at Tirunelveli, we have considered all 525 days (376 Q-days and 149 D-days) with FESF in our further study. Figures 5, 6, and 7 discussed in the following sections represent the statistics based on these 376 Q-days and 149 D-days under FESF category.

4.1. Start and End Time of Active Phase of FESF

Here, we present the statistics of start time (t_1) and end time (t_2) during which $C_I(x_0, t_m) \leq 0.7$ for a given day. The distribution of t_1 and t_2 for Q-days and D-days is depicted in Figure 5. The average values of t_1 and t_2 are $\langle t_1 \rangle = 20.3 \pm 1.7$ and $\langle t_2 \rangle = 21.3 \pm 2.1$ ($\langle t_1 \rangle = 21.3 \pm 2.5$ and

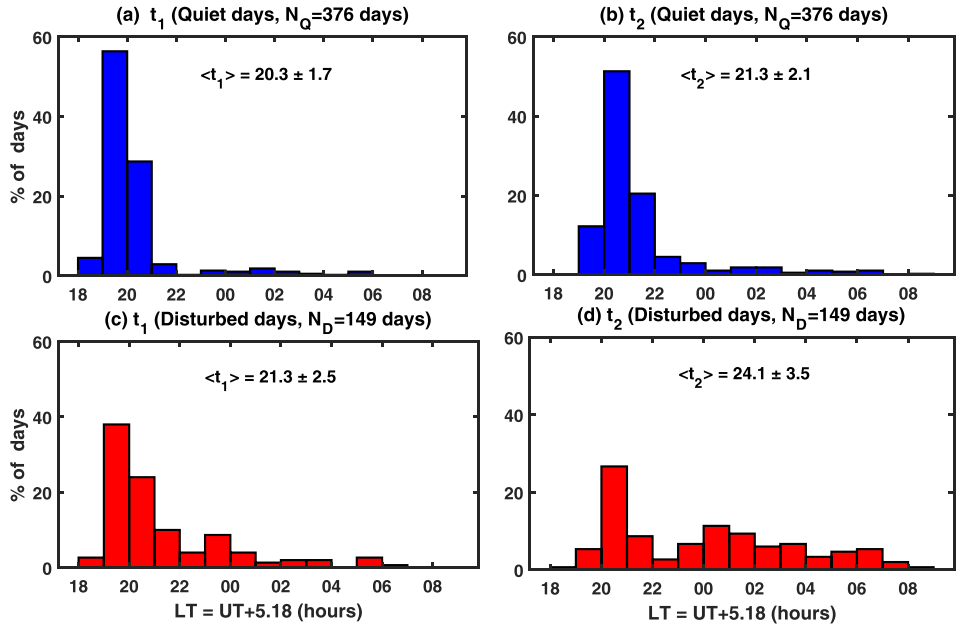

Figure 5. Distribution of t_1 and t_2 (in hours LT) for D-days and D-days. The time of first and the last occurrence of $C_I(x_0, t_m) \leq 0.7$ for a given day are referred to as t_1 and t_2, respectively. On few Q-days, t_1 and t_2 are greater than 22 LT. These events are mainly associated with midnight or early morning FESF occurrence during solstice months.

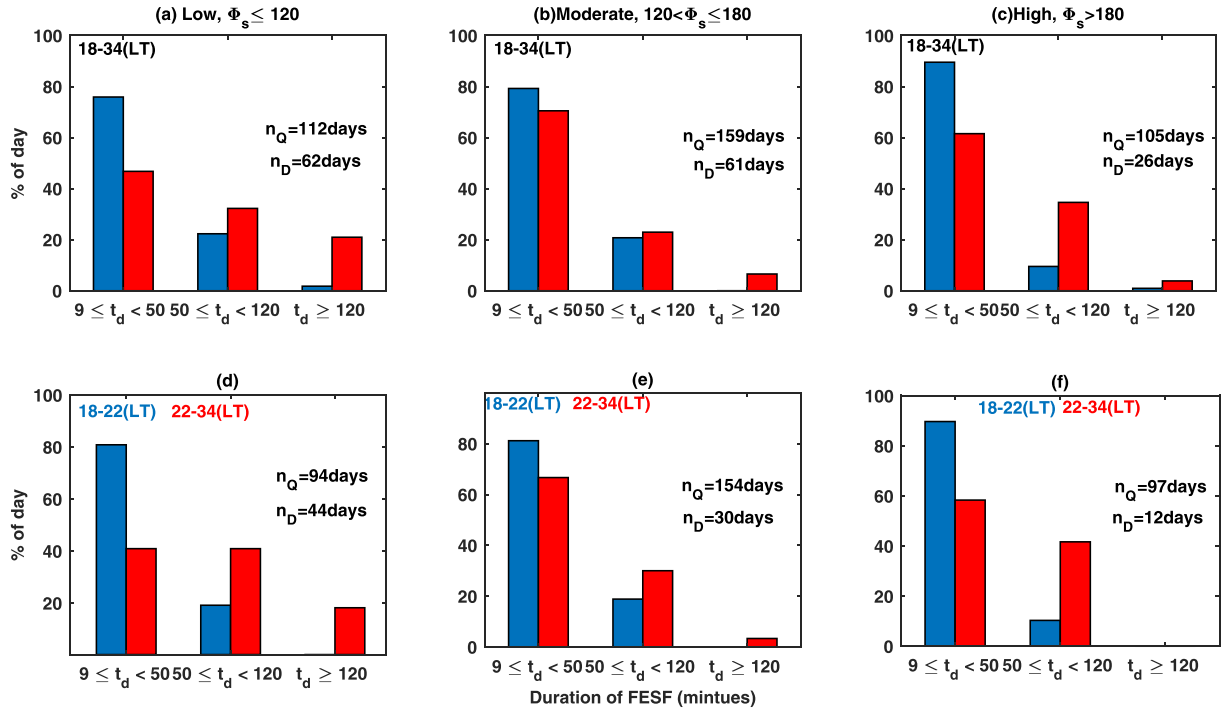

Figure 6. Percentages of days having active phase durations (t_d, in minutes) in three different bins are shown for low ($\Phi_s \leq 120$), moderate ($120 < \Phi_s \leq 180$), and high ($\Phi_s > 180$) solar flux periods. These percentages are shown in panels (a–c) for 18–34 LT for quiet (blue) and disturbed (red) days, whereas percentages shown in panels (d–f) correspond to 18–22 LT for Q-days (blue) and 22–34 LT for D-days (red). Here 18–34 LT represents the time from 18 LT on the nth day until 10 LT on the $n+1$th day.

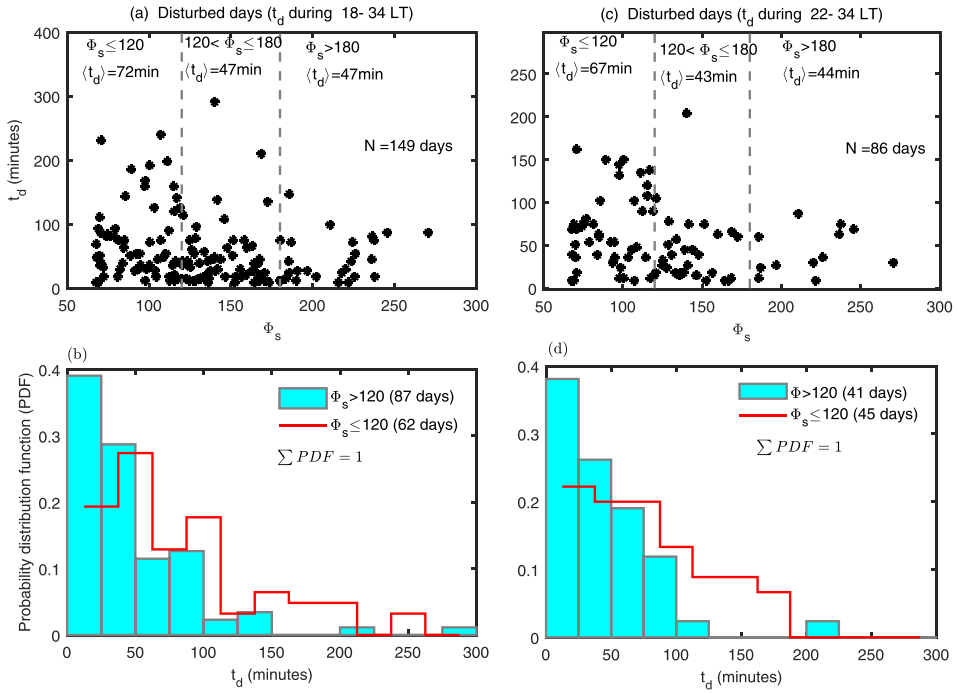

Figure 7. Active phase duration as a function of solar flux for D-days during (a) 18–34 LT and (c) 22–34 LT are shown. The corresponding average active phase duration during low ($\Phi_s \leq 120$), moderate ($120 < \Phi_s \leq 180$), and high ($\Phi_s > 180$) solar activity are mentioned in panels (a) and (c). Two vertical dotted lines in panels (a) and (c) represent $\Phi_s = 120$ and $\Phi_s = 180$. Here 18–34 LT represents the time from 18 LT on the nth day until 10 LT on the $n+1$th day. The probability distributions of t_d during (b) 18–34 LT and (d) 22–34 LT are shown for low ($\Phi_s \leq 120$; red color) and moderate–high ($\Phi_s > 120$; cyan color) solar flux periods.

$\langle t_2 \rangle = 24.0 \pm 3.5$), respectively for Q-days (D-days). These values are mentioned in their respective subplots in Figure 5. For Q-days, if we add percentages shown in Figure 5a or 5b, we will get 100%, which corresponds to 376 days. Similarly, for D-days, if we add percentages shown in Figure 5c or 5d, we will get 100%, which corresponds to 149 days. It may be noted that for Q-days, both t_1 and t_2 mainly lie in the post-sunset, pre-midnight period (i.e., <22 LT). For majority (≈85%) of days, t_1 lies approximately in the range of 19–21 LT and t_2 lies in the range of 20–22 LT. It is as expected because on Q-days, the fresh generation of EPBs mostly takes place around post-sunset hours generally, after 19 LT (Bhattacharyya et al., 2003; Smith & Heelis, 2017). We also see that t_1 and t_2 occasionally exceed 22 LT on few Q-days (28 days). These days are associated with midnight or post-midnight generation of EPBs related to the solstice months (Niranjan et al., 2003; Smith et al., 2016) and some are associated with early morning generation of EPBs (Kil et al., 2019). These 28 days with midnight and early morning FESF irregularities on Q-days are found to be associated with mainly weak (61%) and to some extent with moderate scintillations (30%). On the other hand, for magnetically D-days, the distribution of t_1 and t_2 shows different scenario. The occurrence of t_1 and t_2 is probable even after 22 LT on magnetically D-days. It indicates that the generation of EPBs is equally favored around midnight and post-midnight hours on magnetically D-days, which is in agreement with earlier studies (Abdu, Batista, et al., 2003; Bhattacharyya et al., 2002; Fejer & Scherliess, 1997; Huang et al., 2005; Li et al., 2010; Richmond et al., 2003). This behavior is attributed to the westward to eastward turning of zonal electric field due to magnetic activity-linked electric fields, which get superimposed on ambient F region electric fields. Based on the level of 10.7-cm solar flux (Φ_s), we have divided these FESF Q-days and D-days into three categories, namely, low ($\Phi_s \leq 120$), moderate ($120 < \Phi_s \leq 180$), and high ($\Phi_s > 180$) solar flux. In the next subsections, we are elaborating the effect of solar flux and geomagnetic activity on active phase duration of FESF for these 525 days.

4.2. Distribution of Active Phase Duration of FESF

As discussed in the previous section, we have estimated the average active phase duration (t_d) of the FESF irregularities, when the perturbation electric field associated with EPBs drifting over Tirunelveli is considered to be alive. In general, t_d varies in the range of 9–210 and 9–291 min for Q-days and D-days, respectively.

Based on this range, we have chosen three bins for t_d so that each bin has reasonable number of days. The percentage of days having t_d in different bins (viz., 9–50, 50–120, and >120 min) is estimated for low, moderate, and high solar flux categories as shown in Figure 6. In this figure, the upper panels (Figures 6a–6c) correspond to estimates of t_d during 18–34 LT for low, moderate, and high solar flux periods, respectively. The number of days under each category is mentioned in respective subplots. It may be noted that for each subplot representing low/moderate/high solar activity, if we add percentage of days under different bins of t_d, then we will get 100%, which corresponds to total number of days with FESF under given category (i.e., Q-days/D-days) with that level of solar activity. For example, in Figure 6a, if we add percentages shown by all blue (red) bars, then we will get number of Q-days (D-days) with FESF during low solar flux and it is $n_Q = 112$ days ($n_D = 62$ days). Similarly, for moderate and high solar flux periods, the number of Q-days (D-days) is $n_Q = 159$ days and $n_Q = 105$ days ($n_D = 61$ days and $n_D = 26$ days), respectively.

The evident tendency seen in Figure 6 is that the active phase duration of FESF is longer on D-days as compared to that on Q-days. Such tendency is reported recently by Gurram et al. (2018); however, this statistical feature is not examined separately for different levels of solar flux as presented in Figure 6. On Q-days, the majority of days are having t_d in the range of 9–50 min, and occasionally, it is 50–120 min, whereas on D-days, considerable number of days are having active phase durations larger than 50 min. Overall, the average active phase duration are $\langle t_d \rangle = 57.9 \pm 52.3$ min for D-days and $\langle t_d \rangle = 33.8 \pm 23.4$ min for Q-days. For both Q-days and D-days, the standard deviation in average t_d is high as it spans large range starting from 9 to 291 min, which is attributed to day-to-day variation in the evolution of FESF. Also, on D-days, the average t_d includes the active phase duration of the usual post-sunset ESF, which may or may not be related to magnetic activity. It may be noted that for D-days, we have now purposely excluded the period of 18–22 LT and depicted the distribution of t_d in the lower panels of Figure 6. It is because, usually, on Q-days, the FESF is seen in the post-sunset hours, and as a result, lower values of $C_I(x_0,t_m)$ are observed in the early phase (<22 LT). However, on D-day, its occurrence is not restricted to only post-sunset hours. Hence, on D-days, what we see during 18–22 LT may or may not have been triggered by magnetic activity. It means that the identification of magnetic activity-linked FESF during 18–22 LT is difficult. In such scenario, we cannot be sure whether the FESF seen during 18–22 LT has any association with magnetic activity or not (Bhattacharyya et al., 2002). Thus, we estimated the $\langle t_d \rangle$ by utilizing active phase durations during 22–34 LT for D-days and 18–22 LT for Q-days, which is shown in Figures 6d, 6e, and 6f for low, moderate, and high solar flux periods, respectively. In this case, the average active phase duration of FESF comes out to be 55.7 ± 42.1 min for D-days and 32.3 ± 19.5 min for Q-days. It suggests that even if we exclude the FESF duration before 22 LT while computing t_d for D-days, the tendency of association of longer active phase duration of FESF on magnetically D-days is intact and it is consistent for all levels of solar flux. We know that during low solar activity solstice months, the midnight FESF is common even on Q-days. Thus, we verified the tendencies seen in Figures 6a and 6d particularly by taking the period of 22–34 LT for both Q-days and D-days of solstice. In this case, the $\langle t_d \rangle$ is found to be 34.5 ± 28.9 for Q-days and 67.5 ± 43.8 for D-days, which implies that observed tendencies are applicable to low solar flux solstice period as well.

From Figure 6, we observe that for Q-days, the percentage of days having $t_d \geq 50$ min is found to be 24%, 20.8%, and 10.5% (corresponding to 27, 33, and 11 days). And if we exclude midnight and early morning FESF events, then these percentages change to 19.2%, 18.8%, and 10.3% (corresponding to 18, 29, and 10 days) for low, moderate, and high solar flux periods, respectively. For D-days, the percentage of days having $t_d \geq 50$ min is found to be 53.2%, 29.5%, and 38.5% (corresponding to 33, 18, and 10 days) during low, moderate, and high solar flux periods, respectively. If we exclude the FESF period before 22 LT for magnetically D-days, then these percentages change to 58%, 33.3%, and 41.7% (corresponding to 25, 10, and 5 days) for low, moderate, and high solar flux periods, respectively. In fact, the days with $t_d > 120$ min are predominantly seen during magnetically D-days of low solar activity. On D-days, the longer durations of active phase of FESF have greater probability of occurrence during low solar activity, and this statistical tendency is based on sufficient number of magnetically D-days (i.e., ≈33–58%). However, for Q-days, it is difficult to conclude about such solar flux dependence in the post-sunset hours (18–22 LT) as we have less number of days with longer active phase duration of FESF (i.e., ≈10–19%).

To understand this feature better, in Figure 7a, we have shown variation of t_d as a function of solar flux for D-days. In this figure, the vertical dashed lines mark three regions of solar flux, namely, $\Phi_s \leq 120$, $120 < \Phi_s \leq 180$, and $\Phi_s > 180$. It may be noted that the longer active phase durations of FESF are mostly populated in low solar flux period. The average value of active phase duration of FESF for these three bins

of solar flux are mentioned in the plot and they are $\langle t_d \rangle = 72 \pm 58$, $\langle t_d \rangle = 47 \pm 49$, and $\langle t_d \rangle = 47 \pm 35$ min for low, moderate, and high solar flux periods, respectively. The average t_d is relatively smaller for moderate to high solar flux as compared to low solar flux period. Thus, we have shown the probability distribution function (PDF) of t_d for low ($\Phi_s \leq 120$) and moderate–high ($\Phi_s > 120$) solar flux periods in Figure 7b. Here, summation of PDF is 1 (i.e., 100%), and it corresponds to total number of days under respective categories. The difference in the PDF of t_d during low (red color) and moderate–high (cyan color) solar flux periods is clearly visible. Both Figures 7a and 7b suggest the tendency of presence of longer active phase duration of FESF during low solar activity. Even if we include FESF periods occurring only after 22 LT while computing t_d, this tendency persists for magnetically D-days, which is clearly seen in Figures 7c and 7d. It may be noted that in Figures 7a and 7b, we have total 149 D-days, and in Figures 7c and 7d, we have 86 days. It is because there are 63 D-days on which FESF was seen only during 18–22 LT. We find that the PDFs of t_d associated with low and moderate–high solar flux periods are different and this tendency holds irrespective of the choice of time interval chosen for the computation of t_d (i.e., 18–34 and 22–34 LT). Hence, we can confirm likeliness of longer active phase of the FESF on D-days during low solar activity periods.

As seen in Figures 6 and 7, there is a large spread in the values of t_d for D-days. Each D-day is different, and their start time, duration, strength, local time, and interplanetary solar wind conditions responsible for the magnetic activity differ from one D-day to another. We have compiled active phase duration of FESF resulting from magnetic activity-linked electric fields. We have significant number of days, and in such statistical study, the first step is to check the level of magnetic activity on these D-days. It may provide us additional information to understand the variation of duration of active phase of FESF associated with magnetic activity. For Q-days, mostly the t_d is less than 50 min and the average t_d comes out to be 33.8 min. Thus, we have examined all FESF D-days with $t_d \geq 35$ min (total 87 days), and their details are elaborated in the next section.

4.3. Role of Geomagnetic Activity

The disturbance dynamo (DD) and prompt penetration (PP) electric fields are the two main sources of modulation of ionospheric electric field during magnetic activity. These magnetic activity-linked electric fields (DD/PP/DD + PP) can either suppress or initiate the generation of EPBs depending on their direction, strength, and spatial structures in the equatorial *F* region. Here, our aim is not to explore the reasons behind the occurrence/non-occurrence of FESF. In fact, we have chosen all days with occurrence of FESF. It means that the ionospheric conditions were favorable for the generation of ESF. If generation of FESF is triggered by magnetic activity-linked electric field modulations in the *F* region, then for how long would the active phase of FESF last? We are trying to address this question here. We have chosen commonly used parameters like IMF, IEF, *SYMH* index, a measure of ring current, and *Kp* index to track the magnetic activity on D-days. In general, IMF *Bz* plays an important role in determining the strength of geomagnetic storm that is manifested in the *SYMH* index (Gonzalez & Echer, 2005; Kane & Echer, 2007). Apart from this, time variation of IEF E_y is examined, which gives the magnitude of the convection electric field present at the Earth's magnetopause. Here, positive E_y represents dawn-to-dusk IEF, which is eastward on dayside. So, IMF *Bz*, IEF E_y, *SYMH*, and *Kp* are reasonable proxies that can be used to track the level of magnetic activity.

Although t_1 is the time when presence of perturbation electric field associated with EPBs first gets manifested in the $C_I(x_0, t_m)$, we observe active phase until time t_2. This active phase may be associated with single or multiple FESF resulting from magnetic activity-linked electric fields at different time during the night. If magnetic activity-linked electric fields support generation of ESF, then development of such density structures will take some time. As these electron density structures decay slowly through diffusion, we can still observe scintillations after time t_2, but certainly, there is negligible perturbation electric field beyond time t_2. It suggest that observed FESF is associated with the magnetic activity-linked modulations in the low latitude *F* region occurring prior to $t_2 - 30$ min. Here the lag of 30 min is considered as time required for development of ESF irregularities that produce scintillations would take some time after the low latitude *F* region electric field is altered due to magnetic activity. Hence, for a given *n*th day, we have examined the variation of IMF *Bz*, E_y, *SYMH*, and *Kp* from 00 LT of *n*th day until time $t_{effect} = t_2 - 30$. On magnetically disturbed day, the FESF is likely to be seen around midnight or post-midnight hours. Thus, t_{effect} is often found to be in the early hours of $n + 1$th day (i.e., 00–04 LT on $n + 1$th day). During this examination, we have noted the occurrence of minima in IMF *Bz*, maximum in IEF E_y, minimum in *SYMH*, and maximum in *Kp*. Also, their respective time of occurrence t_{min}^{Bz}, t_{max}^{Ey}, t_{min}^{SYMH}, and t_{max}^{Kp} are noted. The minima in IMF *Bz* and *SYMH*

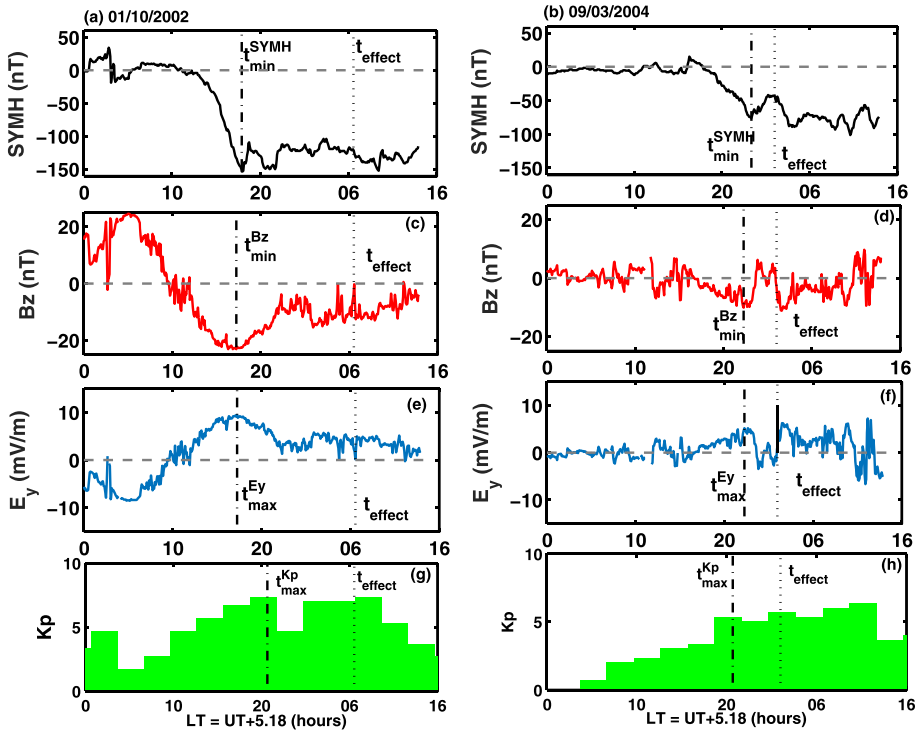

Figure 8. As an example the variation of (a,b) *SYMH*, (c,d) IMF *Bz*, (e,f) IEF *Ey* and (g,h) *Kp* are plotted as a function of local time for two magnetically D-days namely, 1 October 2002 and 9 March 2004, respectively. On x-axis 0 and 30 respectively represent 00 LT of *n*th day and 06 LT of $n+1$th day. The scintillations may be observed between 18 LT of *n*th day to 08LT of $n+1$th day. The time t_{effect} are shown by vertical dashed lines. The time of minimum in *SYMH*, minimum in IMF *Bz*, maximum in *Ey*, and maximum in *Kp* prior to time t_{effect} are shown by dashed-dotted lines in respective plots.

or maximum in IEF *Ey* and *Kp* provide estimates of maximum deviations in proxy measures of geomagnetic activity prior to time t_{effect}. We have taken $|Bz_{min}|$, $|SYMH_{min}|$, Ey_{max}, and Kp_{max} as the proxy measures for the strength of magnetic activity.

As examples, the time variations of *SYMH*, IMF *Bz*, IEF *Ey*, and *Kp* for 2 days (1 October 2002 and 9 March 2004) are shown in Figure 8. These two events are chosen as examples because the local time variations of $C_I(x_0, t_m)$ for these two events are depicted in Figures 2c and 2d. The time t_{effect} and time of occurrence of minimum in IMF *Bz* and *SYMH* and maximum in IEF *Ey* and *Kp* are shown by vertical dotted lines in respective subplots in Figure 8. We followed similar analysis for all 87 D-days, which are having $t_d \geq 35$ min, and obtained the above-mentioned proxy parameters to track the level of magnetic activity.

Now, let us briefly discuss the 1 October 2002 case shown in in Figure 8. The IMF *Bz* turned southward ~11 LT and the minima occurred around 17.3 LT. The IEF *Ey* is strong and it is eastward during the entire period of 11–22 LT (see Figure 8e). The PP is generally seen nearly simultaneously at low latitudes (Fejer et al., 1990; Forbes et al., 1995; Kikuchi et al., 2000; Spiro et al., 1988), but how long it will keep penetrating is dependent on the strength and variation of magnetospheric convection electric field and its shielding. This eastward convection electric field can penetrate to low latitudes until ~22 LT (Nopper Jr & Carovillano, 1978). Sometimes, IMF *By* also plays a role in determining the PP of electric field (Chakrabarty et al., 2017). On the other hand, as magnetic activity is initiated around ~11 LT, DD is already in operation around 18 LT. Generally, DD electric field may arrive at low latitude within 1–12 h (Scherliess & Fejer, 1997). These DD electric fields are expected to be westward around dusk sector and eastward around midnight and post-midnight hours. Also, Joule heating at high latitude that is responsible for setting the DD is expected to be highly variable and dependent on the level of magnetic activity. Thus, depending on magnetic activity, the observed FESF on a given night could be associated with either PP or DD or complex combination of both these electric fields.

Next, we have shown the time of occurrence of minimum in IMF *Bz*, maximum in IEF *Ey*, minimum in *SYMH*, and maximum in *Kp* as a function of t_d in Figures 9a, 9b, 9c, and 9d, respectively. The PDFs of $|Bz_{min}|$,

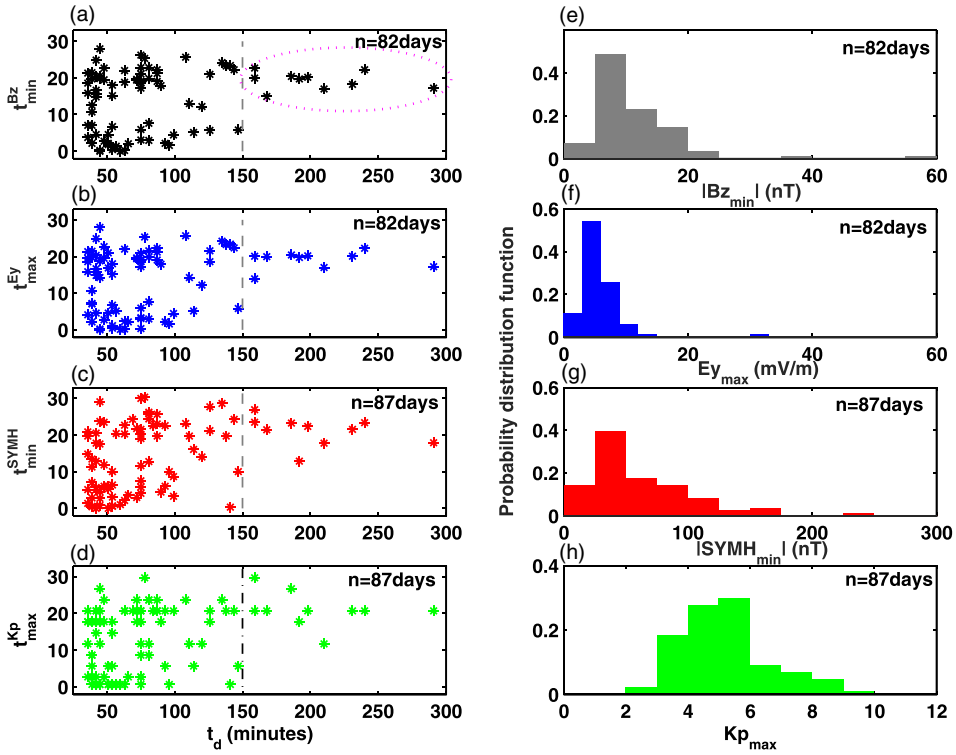

Figure 9. (a–d) The time of occurrence of Bz_{min}, Ey_{max}, $SYMH_{min}$, and Kp_{max} are shown as a function of t_d. Here, 0 on y axis represents the 00 LT of nth day and 30 represents 06 LT of $n+1$th day. Mainly, the scintillations are observed from 18 LT of nth day to 08 LT of $n+1$th day. The vertical dashed line in (a–d) indicates limit of $t_d = 150$ min and elongated dotted circle in panel (a) represents the cases with $t_d > 150$ min. (e–h) Probability distribution function of $|Bz_{min}|$, Ey_{max}, $|SYMH_{min}|$, and Kp_{max}. In panels (a) and (b), the total number of days is 82 as there is a data loss in IMF Bz for 5 days.

Ey_{max}, $|SYMH_{min}|$, and Kp_{max} for these 87 D-days are depicted in Figures 9e, 9f, 9g, and 9h, respectively. It may be noted that for 5 days, there was a data loss in IMF Bz for more than 4 h prior to t_{effect}, so we could not get Bz_{min}, t^{Bz}_{min}, t^{Ey}_{max}, and Ey_{max} for these days. Thus, we have a total of 82 points in Figures 9a, 9b, 9e, and 9f. The PDFs shown in Figures 9e–9h suggest that the majority of these magnetically D-days are associated with $|Bz_{min}|\sim$ 5-20 nT, $Ey_{max}\sim$ 3-9 mV/m, $|SYMH_{min}|$ ~30–150 nT and Kp_{max} ~4–7. It may be noted that summation of the PDF shown in Figures 9e–9h gives 1 (i.e., 100%), which corresponds to total number of days under respective categories. Interesting feature seen here is related to the days with $t_d > 150$ min, which is marked by the elongated dotted circle in Figure 9a. The vertical dashed line in Figures 9a–9d represents $t_d = 150$ min. Careful scrutiny of these subplots indicates that when $t_d > 150$ min, the minimum in IMF Bz occurs close to afternoon-dusk sector (i.e., $t^{Bz}_{min} \approx$14.9 to 22.7 LT). It suggests that turning of IMF Bz in the close vicinity of afternoon to sunset time is likely to support very long (>150 min) durations of active phase of FESF generated as a result of magnetic activity-linked electric fields (DD/PP/DD + PP). The values of $|Bz_{min}|$ and Ey_{max} for these 10 cases are in the range of 8–38 nT and 4–31 mV/m, respectively.

For better understanding of these longer active phase of EPBs, we have plotted time variation of $C_I(x_0, t_m)$ in Figure 10 for these 10 cases having $td > 150$ min. The usual post-sunset generation of EPBs on Q-days is seen during 18–22 LT, whereas on magnetically D-days, it can extend beyond these hours. So, we examined the contribution to t_d from 18 to 22 LT and 22 to 34 LT, which is mentioned in respective panels in Figure 10. For example, for 7 April 1995, $t_d = 72 + 159 = 231$ min, where 72 and 159 min give contribution to t_d from 18 to 22 LT and 22 to 34 LT, respectively. Similarly, for 1 October 2002, $t_d = 87 + 204 = 291$ min. In general, for these 10 cases, the active phase duration of FESF during 18–22 LT, which is the usual time for the generation of ESF, is also very long (36–144 min). We find that on Q-days, the active phase duration of ESF generated in the usual post-sunset hours is mostly smaller than 40 min (nearly 78%), and occasionally, it only exceeds 50 min (<15%), whereas for these 10 cases, the active phase duration of ESF during 18–22 LT is mostly above 40 min (total seven cases). It may be noted that for 2 days, active phase duration during 18–22 LT is 36 min

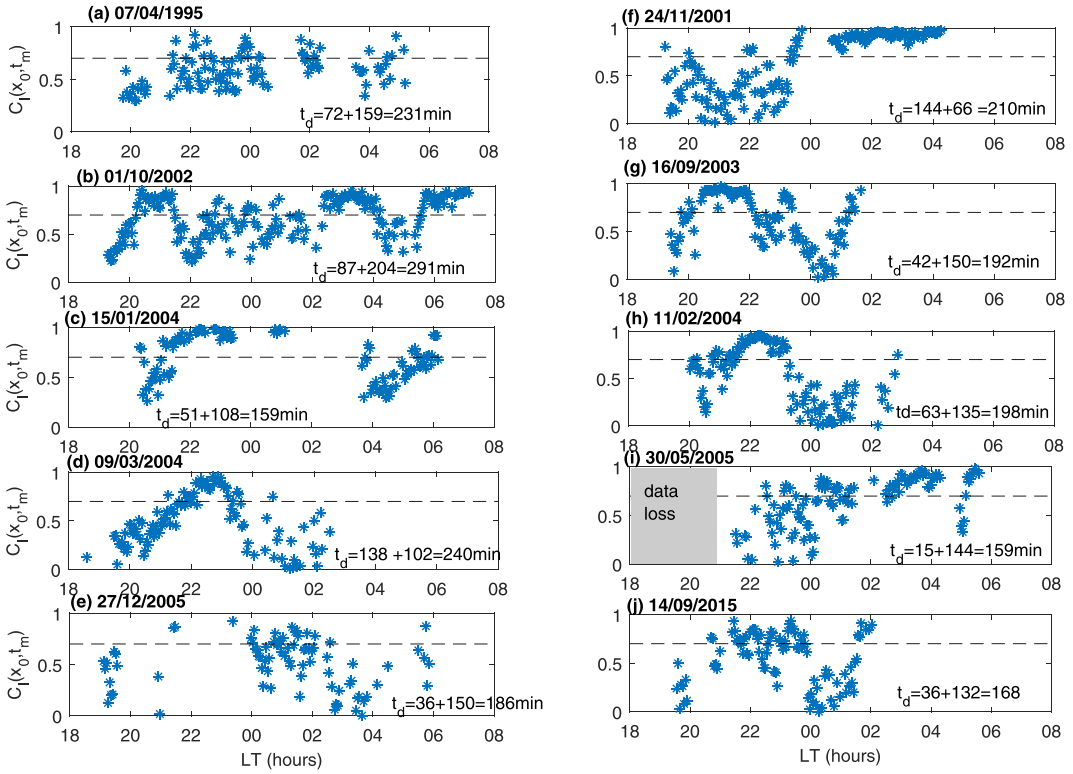

Figure 10. Variation of $C_I(x_0, t_m)$ as a function of local time is shown for 10 magnetically D-days where $t_d > 150$ min. The active phase durations of FESF 18–22 LT and 22–34 LT are mentioned in respective panels. For 7 April 1995, that is, panel (a), the $t_d = 72 + 159 = 231$ min, where 72 and 159 minutes give contribution to t_d from 18 to 22LT and 22 to 34 LT, respectively.

(see Figures 10e and 10j), and for 1 day, it is 15 min (see Figure 10i). The later case for which it is 15 min (i.e., 30 May 2005), there was a data loss during 18–21 LT hours, so we cannot confirm the presence/absence of scintillations during this time. Thus, we can say that the extended active phase of EPBs in the post-sunset hours happens to be the common feature for these 10 cases. In addition, we noticed that for these cases, the generation of ESF is continued after 22 LT and their active phase durations are also longer, that is, in the range of 66–204 min. As the contribution to active phase of FESF from both 18–22 LT and 22–34 LT is sufficiently long, these days happen to be associated with unusually long ($t_d > 150$ min) active phase of EPBs.

In general, each geomagnetic activity episode is unique in nature. For example, there can be one or more southward/northward turnings, the change in IMF *Bz* can be gradual or sharp, and so on. Depending upon the strength of magnetic activity, its time variation and local time effects seen in equatorial *F* region can be associated with either DD or PP or combination of both. These longer active phase durations are a result of the extended evolving phase of EPBs in the usual post-sunset hours. This could likely be caused by the PP of convection electric field of magnetospheric origin close to afternoon–evening local time sector. It is suggested that the PP electric field can be seen without significant attenuation for many hours during the main phase of geomagnetic storms (Huang et al., 2005). Modeling studies have also shown that the timescale of the order of 3,300 min, depending on magnetospheric plasma properties and ionospheric conductivity, is involved in the shielding of this convection electric fields (Richmond et al., 2003). This PP electric field can significantly modify the usual pre-reversal enhancement (PRE) electric field in the evening sector, where prevailing E region horizontal conductivity gradient exists. As a result, we can have extended longer active phase of FESF in the post-sunset period. Also, the FESF around midnight or post-midnight hours observed on these nights might be associated with DD electric field, which is eastward around midnight hours (Huang et al., 2005) and it takes some time (1–12 h) to arrive at the low latitude ionosphere (Scherliess & Fejer, 1997).

Next, we checked the relation between active phase duration of FESF and strength of geomagnetic activity. For this purpose, we plotted t_d as a function of (i) $|SYMH_{min}|$, (ii) $|Bz_{min}|$, (iii) Ey_{max}, and (iv) Kp_{max} in Figures 11a, 11b, 11c, and 11d, respectively. It may be noted that a single value of $|SYMH_{min}|$, $|Bz_{min}|$, Ey_{max},

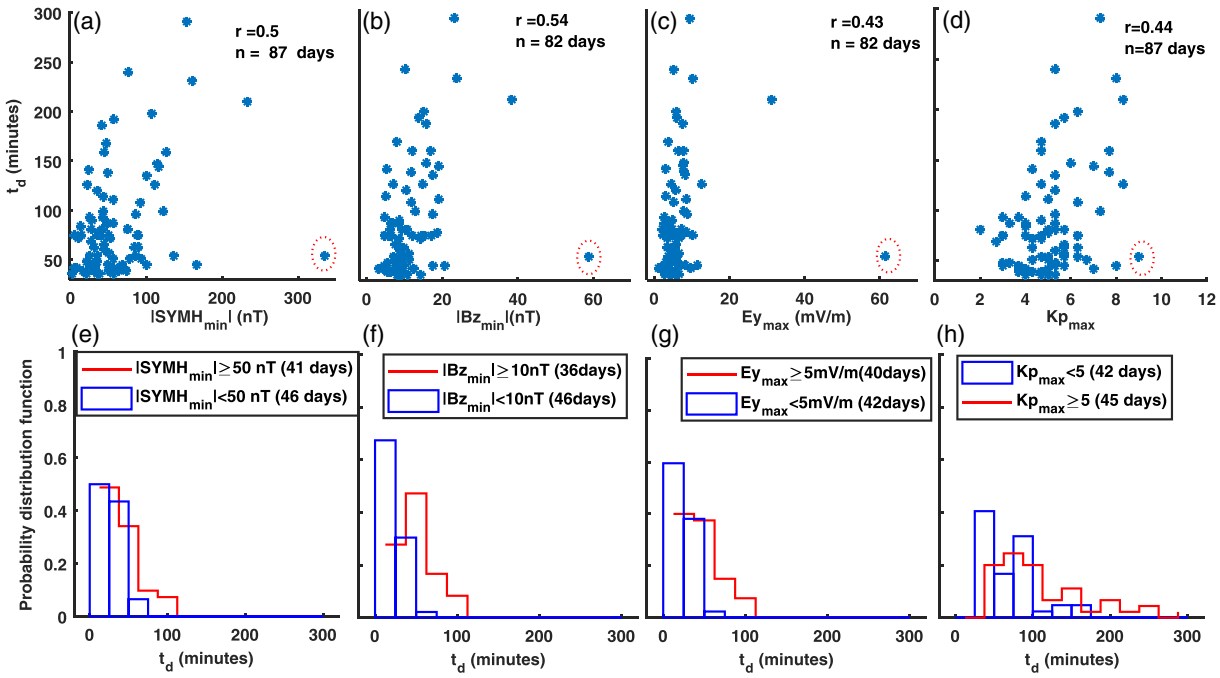

Figure 11. The active phase duration of FESF observed at Tirunelveli as a function of (a) $|SYMH_{min}|$, (b) $|Bz_{min}|$, (c) Ey_{max}, and (d) Kp_{max}. The $|Bz_{min}|$, $|SYMH_{min}|$, Ey_{max}, and Kp_{max} are considered as a proxy to measure the strength of geomagnetic activity for magnetically D-days on which the generation of FESF is observed. Here, we have total 87 days for which $t_d \geq 35$ min. For 2 days, IMF Bz data are not available, and for 3 days, there is a data gap of more than 4 h prior to time t_{effect}. So we have total 82 days in panels (b) and (c). The probability distribution functions of t_d for two levels of (e) $|SYMH_{min}|$, (f) $|Bz_{min}|$, (g) Ey_{max}, and (h) Kp_{max} are shown.

and Kp_{max} is not used to get information about PP or DD electric field. We have used these values just to track the level of magnetic activity that is giving rise to FESF by altering ambient F region electric fields on a given D-day. It is found that active phase durations are positively correlated with $|SYMH_{min}|$, $|Bz_{min}|$, IEF Ey_{max}, and Kp_{max}, and the respective correlation coefficients are 0.50, 0.54, 0.43, and 0.44. There is only one outlier point in Figures 11a–11d which is not considered while computing these correlations. These correlations are 99% statistically significant and based on 82–87 D-days with FESF. In Figures 11e, 11f, 11g, and 11h, we have shown the PDF of t_d for these 82–87 days for two levels of $|SYMH_{min}|$, $|Bz_{min}|$, Ey_{max}, and Kp_{max}, respectively. These PDFs are estimated for two levels of magnetic activity to understand the distribution of t_d for different level of magnetic activity. The PDFs are shown for $|SYMH_{min}| \geq 50$ nT (red color) and $|SYMH_{min}| < 50$ nT (blue color) in Figure 11e. Similarly, for IMF $|Bz_{min}|$, Ey_{max}, and Kp_{max}, the limit of 10 nT, 5 mV/m, and 5 are chosen, respectively (see Figures 11f–11h). A clear shift in the PDF of t_d is apparent for higher values of IMF $|Bz_{min}|$, Ey_{max}, and Kp_{max}. It suggests that stronger geomagnetic storms are likely to produce longer active phase durations for FESF triggered as a result of magnetic activity-linked electric field modulations in the F region. It is possible that perturbation electric field associated with FESF remains alive for more time due to higher height of the equatorial F region or there could be multiple generations of EPBs as a result of magnetic activity-linked electric fields (PP/DD/PP + DD) arriving at different local time. Under both these scenarios, the daily total active phase duration of FESF will be longer. In the next section, we discuss the possible physical mechanisms that can explain the observed tendencies.

5. Discussion

We have estimated active phase duration of the FESF for Q-days and D-days and examined their solar flux and geomagnetic activity dependence in detail. The first evident tendency which is seen here is the presence of longer active phase duration of FESF on D-days as compared to Q-days and it is seen for all levels of solar flux. It may be noted that active phase duration of FESF will be determined by the growth and decay of perturbation electric field associated with the nonlinearly evolving EPBs. Theoretical and simulation studies have reported that the growth time of GRT plasma instability is approximately 10–50 min (Kelley et al., 1979; Yokoyama, 2017). These estimates are based on the linear growth rate of GRT plasma instability; however,

when scintillations are observed, EPBs are already in the nonlinear state. The estimates of active phase durations of EPBs reported in the present study for Q-days (i.e., $\langle t_d \rangle = 33.8 \pm 23.4$ min) are associated with the nonlinear growth and decay phase of EPBs. We know that the ambient ionospheric electric field plays a crucial role in the growth of GRT plasma instability (Kelley et al., 1981). On magnetically disturbed day, the DD and PP electric fields are the major sources for the modulation of ambient ionospheric electric field (Blanc & Richmond, 1980; Kikuchi et al., 2000). If magnetic activity-linked eastward electric field survives for the longer time and it is strong enough to change the ambient westward electric field to eastward, then resultant electric field ($E_{net} = E_{quiet} + E_{disturbed}$) can raise F region to higher altitude. Such higher altitudes can help in sustaining positive growth of the GRT plasma instability. This can lead to a longer active phase of FESF on D-day. Thus, the longer durations of active phase of FESF are partly attributed to the disturbed time ionospheric electric field (i.e., DD or PP or combination of both).

Other feature is the likeliness of longer active phase of FESF during low solar flux period on D-days. It may be noted that the nonlinear evolution of GRT plasma instability affects the time variation of associated perturbation electric field and it will get reflected in estimated t_d. Also, how long the net ambient electric field can support the growth of the GRT plasma instability will be decided by how long the resultant (E_{net}) ambient electric field is eastward. Now the strength and direction (eastward/westward) of resultant ambient electric field are decided by both (i) ambient quiet time electric field and (ii) disturbed time electric field. During high solar flux periods, the ambient electric fields are stronger as compared to low solar flux periods. Earlier studies have reported that the post-PRE maximum westward electric field increases with solar flux (Hysell & Burcham, 2002; Kakad et al., 2012b). It suggests that around midnight and post-midnight hours, where the magnetic activity-linked FESF is prevalent, the ambient quiet time westward electric field is also weaker during low solar activity. Thus, one can say that the magnetic activity-linked electric fields that get superimposed on ambient F region electric field result in a net electric field that remains eastward for a longer time during low solar flux days as compared to high solar flux days. Using ionosonde observations, Kakad et al. (2011) have shown that the effect of magnetic activity-linked DD electric field sustains for longer duration during low solar flux periods. Thus, we propose that the tendency of presence of longer active phase duration of FESF on magnetically D-days during low solar flux period is attributed to the magnetic activity-linked electric field, which can cause net electric field to remain eastward for longer time due to weaker ambient F region electric fields during low solar flux periods.

Although ambient quiet time ionospheric conditions (electric fields, conductivities densities, etc.) are mainly controlled by solar flux, the characteristics of magnetic activity-linked electric fields like strength, time variation, and spatial extent can be highly variable depending upon the nature of geomagnetic activity itself. We find that the FESF generated on D-days with stronger magnetic activity tend to possess longer active phase. The limits for the higher magnetic activity in terms of proxy measures appear to be $Ey_{max} \geq 5$ mV/m, $|Bz_{min}| \geq 10$ nT, $|SYMH_{min}| \geq 50$ nT, and $Kp_{max} \geq 5$. These numbers do not give any direct information about DD or PP electric field strength or duration. It only provides information about level of magnetic activity. But Joule heating at high latitude, which is responsible for setting DD, and PP electric fields are expected to be highly variable and dependent on the level of geomagnetic activity. Thus, the difference in the distribution of t_d for D-days having different levels of magnetic activity is expected (see Figure 11). It suggests the presence of longer active phase of the FESF during higher magnetic activity.

We have also noticed that when maximum southward deviation in IMF Bz happens close to afternoon-dusk sector, there is a likely probability of very long active phase of EPBs ($t_d > 150$ min). These longer active phase durations are a result of extended evolving phase of EPBs in the usual post-sunset hours, likely to be caused by promptly penetrated convection electric field of magnetospheric origin close to afternoon–evening local time sector. In addition, on these nights, there can be FESF around midnight or post-midnight hours due to DD electric field, which is eastward around midnight hours (Huang et al., 2005) and take some time (1–12 h) to arrive at the low latitude ionosphere (Scherliess & Fejer, 1997). Thus, for such cases, the total active phase duration of EPBs happens to be very long as compared to other D-days.

6. Summary and Conclusion

In this paper, we have made an attempt to quantify the duration of evolving or active phase of EPBs during Q-days and D-days. This information is important and it is less explored so far. Active phase basically refers to the phase when perturbation electric field associated with the EPBs drifting over Tirunelveli is alive or not

eroded significantly. Long-term spaced receiver amplitude scintillation observations on 251 MHz are used in the study. We used the parameter $C_I(x_0, t_m)$ to identify the active phase of FESF. We noticed that days with FESF produce more moderate–strong scintillations during the night as compared to days with drifted-in ESF. Recently, Gurram et al. (2018) have reported active phase durations of the FESF observed at dip equatorial station Tirunelveli. However, in their study, they did not investigate the solar flux and geomagnetic activity dependence of active phase of FESF, which we have examined here. It is found that active phase duration of FESF generated on magnetically D-days is longer as compared to Q-days and this tendency is consistent for all levels of solar flux. However, D-days with longer duration of FESF (>50 min) are dominated during low solar flux period. We found that the FESF generated on days with higher magnetic activity tend to possess longer active phase duration. In our statistical study, the limits for the higher magnetic activity come out to be $Ey_{max} \geq 5$ mV/m, $|Bz_{min}| \geq 10$ nT, $|SYMH_{min}| \geq 50$ nT, and $Kp_{max} \geq 5$. In addition, we noticed that if maximum southward deviation in IMF Bz occurs in the close vicinity of afternoon to sunset sector (i.e., $t_{min}^{Bz} \approx 14.9$ to 22.7 LT) and if it triggers FESF, then these EPBs are likely to have very long (>150 min) active phase. The associated $|Bz_{min}|$ and Ey_{max} for these cases are in the range of 8–38 nT and 4–31 mV/m, respectively.

In general, both growth and decay of perturbation electric field associated with the nonlinearly evolving GRT plasma instability contribute to active phase duration of FESF. Background ionospheric electric field plays an important role in determining the nonlinear evolution of GRT plasma instability (Kelley et al., 1981), and hence, it can affect the active phase duration of FESF. The net electric field in the F region is decided by both quiet time ambient electric field and disturbed time magnetic activity-linked electric field. The magnetic activity-linked eastward electric field should be sufficiently strong to reverse the ambient westward electric field to eastward in order to raise the F region height during post-PRE time. It is shown that the post-PRE ambient westward electric field is weaker during low solar flux (Hysell & Burcham, 2002; Kakad et al., 2012b), which facilitate the westward to eastward reversal of net electric field during magnetically D-days. It is shown that duration of eastward DD electric field associated with magnetic activity decreases as solar flux increases (Kakad et al., 2011). Thus, the presence of longer active phase duration of FESF is attributed to persistence of magnetic activity-linked eastward electric fields for longer time due to weaker ambient westward ionospheric electric fields during low solar flux.

Depending on strength and variation of magnetic activity-linked electric fields (PP/DD/PP + DD), the FESF may or may not get triggered on a given night. But if FESF are triggered due to magnetic activity, then there is more probability that the perturbation electric field linked with the FESF survives for longer time during low solar activity. In addition, stronger geomagnetic activity is likely to support the generation of EPBs with longer active phase associated with either single or multiple EPBs during the night. Statistical information provided in this study will be useful to understand the durations of active phase of ESF irregularities generated as a result of magnetic activity.

Data Availability Statement

VHF scintillation experiment data are available online (https://doi.org/10.5281/zenodo.1402938).

Acknowledgments
We thank WDC Kyoto for geomagnetic activity indices (http://wdc.kugi.kyoto-u.ac.jp), CDAWEB team for interplanetary solar wind data (https://cdaweb.gsfc.nasa.gov), and NASA NGDC team for solar flux (https://www.ngdc.noaa.gov). We are thankful to K.U. Nair, K. Jeeva, and Ananthi for the technical support to VHF spaced receiver experiment. A. B. acknowledges Indian National Science Academy for an INSA Senior Scientist position at CSRE, IIT Bombay. VHF scintillation experiment was operated by IIG, New Panvel, India.

References

Abdu, M. A., Batista, I. S., Takahashi, H., MacDougall, J., Sobral, J. H., Medeiros, A. F., & Trivedi, N. B. (2003). Magnetospheric disturbance induced equatorial plasma bubble development and dynamics: A case study in Brazilian sector. *Journal of Geophysical Research*, *108*(A12), 1449. https://doi.org/10.1029/2002JA009721

Abdu, M., de Paula, E. R., Batista, I. S., Reinisch, B. W., Matsuoka, M. T., Camargo, P. O., et al. (2008). Abnormal evening vertical plasma drift and effects on ESF and EIA over Brazil-South Atlantic sector during the 30 October 2003 superstorm. *Journal of Geophysical Research*, *113*, A07313. https://doi.org/10.1029/2007JA012844

Abdu, M., Souza, J., Batista, I., & Sobral, J. (2003). Equatorial spread F statistics and empirical representation for IRI: A regional model for the Brazilian longitude sector. *Advances in Space Research*, *31*(3), 703–716. https://doi.org/10.1016/S0273-1177(03)00031-0

Ajith, K. K., Tulasi Ram, S., Yamamoto, M., Otsuka, Y., & Niranjan, K. (2016). On the fresh development of equatorial plasma bubbles around the midnight hours of June solstice. *Journal of Geophysical Research: Space Physics*, *121*, 9051–9062. https://doi.org/10.1002/2016JA023024

Basu, S., Kudeki, E., Basu, S., Valladares, C. E., Weber, E. J., Zengingonul, H. P., et al. (1996). Scintillations, plasma drifts, and neutral winds in the equatorial ionosphere after sunset. *Journal of Geophysical Research*, *101*(A12), 26,795–26,809. https://doi.org/10.1029/96JA00760

Bhattacharyya, A. (2004). Role of E region conductivity in the development of equatorial ionospheric plasma bubbles. *Geophysical Research Letters*, *31*, L06806. https://doi.org/10.1029/2003GL018960

Bhattacharyya, A., Basu, S., Groves, K. M., Valladares, C. E., & Sheehan, R. (2001). Dynamics of equatorial Fregion irregularities from spaced receiver scintillation observations. *Geophysical Research Letters*, *28*(1), 119–122. https://doi.org/10.1029/2000GL012288

Bhattacharyya, A., Basu, S., Groves, K. M., Valladares, C. E., & Sheehan, R. (2002). Effect of magnetic activity on the dynamics of equatorial F region irregularities. *Journal of Geophysical Research*, *107*(A12), 1489. https://doi.org/10.1029/2002JA009644

Bhattacharyya, A., Fedrizzi, M., Fuller-Rowell, T., Gurram, P., Kakad, B., Sripathi, S., & Sunda, S. (2019). Effect of magnetic storm related thermospheric changes on the evolution of equatorial plasma bubbles. *Journal of Geophysical Research: Space Physics*, *124*, 2256–2270. https://doi.org/10.1029/2018JA025995

Bhattacharyya, A., Franke, S., & Yeh, K. (1989). Characteristic velocity of equatorial F region irregularities determined from spaced receiver scintillation data. *Journal of Geophysical Research*, *94*(A9), 11,959–11,969. https://doi.org/10.1029/JA094iA09p11959

Bhattacharyya, A., Groves, K., Basu, S., Kuenzler, H., Valladares, C., & Sheehan, R. (2003). L-band scintillation activity and space-time structure of low-latitude UHF scintillations. *Radio Science*, *38*(1), 1004. https://doi.org/10.1029/2002RS002711, .

Bhattacharyya, A., Kakad, B., Gurram, P., Sripathi, S., & Sunda, S. (2017). Development of intermediate-scale structure at different altitudes within an equatorial plasma bubble: Implications for L-band scintillations. *Journal of Geophysical Research: Space Physics*, *122*, 1015–1030. https://doi.org/10.1002/2016JA023478

Bilitza, D., Altadill, D., Truhlik, V., Shubin, V., Galkin, I., Reinisch, B., & Huang, X. (2017). International Reference Ionosphere 2016: From ionospheric climate to real-time weather predictions. *Space Weather*, *15*, 418–429. https://doi.org/10.1002/2016SW001593, .

Blanc, M., & Richmond, A. (1980). The ionospheric disturbance dynamo. *Journal of Geophysical Research*, *85*(A4), 1669–1686. https://doi.org/10.1029/JA085iA04p01669

Briggs, B. H (1984). The analysis of spaced sensor records by correlation techniques, in middle atmosphere program. *Handbook for MAP*, *13*, 166–186.

Burke, W., Gentile, L., Huang, C., Valladares, C., & Su, S. (2004). Longitudinal variability of equatorial plasma bubbles observed by DMSP and ROCSAT-1. *Journal of Geophysical Research*, *109*, A12301. https://doi.org/10.1029/2004JA010583

Carter, B., Yizengaw, E., Retterer, J., Francis, M., Terkildsen, M., Marshall, R., et al. (2014). An analysis of the quiet time day-to-day variability in the formation of postsunset equatorial plasma bubbles in the Southeast Asian region. *Journal of Geophysical Research: Space Physics*, *119*, 3206–3223. https://doi.org/10.1002/2013JA019570

Chakrabarty, D., Hui, D., Rout, D., Sekar, R., Bhattacharyya, A., Reeves, G. D., & Ruohoniemi, J. (2017). Role of IMF by in the prompt electric field disturbances over equatorial ionosphere during a space weather event. *Journal of Geophysical Research: Space Physics*, *122*, 2574–2588. https://doi.org/10.1002/2016JA022781, .

Engavale, B., & Bhattacharyya, A. (2005). Spatial correlation function of intensity variations in the ground scintillation pattern produced by equatorial spread-F irregularities. *Indian Journal of Radio and Space Physics*, *34*(1), 23.

Engavale, B., Jeeva, K., Nair, K. U., & Bhattacharyya, A. (2005). Solar flux dependence of coherence scales in scintillation patterns produced by ESF irregularities. *Annales Geophysicae*, *23*(10), 3261–3266. https://doi.org/10.5194/angeo-23-3261-2005

Fejer, B. (1997). The electrodynamics of the low-latitude ionosphere: Recent results and future challenges. *Journal of Atmospheric and Solar-Terrestrial Physics*, *59*(13), 1465–1482. https://doi.org/10.1016/S1364-6826(96)00149-6

Fejer, B. G., & Scherliess, L. (1997). Empirical models of storm time equatorial zonal electric fields. *Journal of Geophysical Research*, *102*(A11), 24,047–24,056. https://doi.org/10.1029/97JA02164

Fejer, B. G., Spiro, R., Wolf, R., & Foster, J. (1990). Latitudinal variation of perturbation electric fields during magnetically disturbed periods-1986 sundial observations and model results. *Annales Geophysicae*, *8*, 441–454.

Forbes, J., Roble, R., & Marcos, F. (1995). Equatorial penetration of magnetic disturbance effects in the thermosphere and ionosphere. *Journal of Atmospheric and Terrestrial Physics*, *57*(10), 1085–1093. https://doi.org/10.1016/0021-9169(94)00124-7

Gonzalez, W., & Echer, E. (2005). A study on the peak dst and peak negative bz relationship during intense geomagnetic storms. *Geophysical Research Letters*, *32*, L18103. https://doi.org/10.1029/2005GL023486

Gurram, P., Kakad, B., Bhattacharyya, A., & Pant, T. (2018). Evolution of freshly generated equatorial spread f (f-ESF) irregularities on quiet and disturbed days. *Journal of Geophysical Research: Space Physics*, *123*, 7710–7725. https://doi.org/10.1029/2018JA025705

Gurram, P., Kakad, B., Ravi Kumar, M., & Bhattacharyya, A. (2019). Earthquake/tsunami-linked imprints in the equatorial F region zonal plasma drifts and spatial structures of plasma bubbles. *Journal of Geophysical Research: Space Physics*, *124*, 504–520. https://doi.org/10.1029/2018JA025798

Huang, C.-S., & Kelley, M. C. (1996a). Nonlinear evolution of equatorial spread F: 1. On the role of plasma instabilities and spatial resonance associated with gravity wave seeding. *Journal of Geophysical Research*, *101*(A1), 283–292. https://doi.org/10.1029/95JA02211

Huang, C.-S., & Kelley, M. C. (1996b). Nonlinear evolution of equatorial spread F: 3. Plasma bubbles generated by structured electric fields. *Journal of Geophysical Research*, *101*(A1), 303–313. https://doi.org/10.1029/95JA02209

Huang, C.-M., Richmond, A., & Chen, M.-Q. (2005). Theoretical effects of geomagnetic activity on low-latitude ionospheric electric fields. *Journal of Geophysical Research*, *110*, A05312. https://doi.org/10.1029/2004JA010994

Hysell, D., & Burcham, J. (2002). Long term studies of equatorial spread F using the JULIA radar at Jicamarca. *Journal of Atmospheric and Solar-Terrestrial Physics*, *64*(12–14), 1531–1543. https://doi.org/10.1016/S1364-6826(02)00091-3

Hysell, D., Kelley, M., Swartz, W., & Woodman, R. (1990). Seeding and layering of equatorial spread F by gravity waves. *Journal of Geophysical Research*, *95*(A10), 17,253–17,260. https://doi.org/10.1029/JA095iA10p17253

Joshi, L. M., Balwada, S., Pant, T., & Sumod, S. (2015). Investigation on F layer height rise and equatorial spread F onset time: Signature of standing large-scale wave. *Space Weather*, *13*, 211–219. https://doi.org/10.1002/2014SW001129

Joshi, L., Tsai, L., Su, S., Otsuka, Y., Yokoyama, T., Yamamoto, M., et al. (2019). Investigation of spatio-temporal morphology of plasma bubbles based on ear observations. *Journal of Geophysical Research: Space Physics*, *124*, 10,549–10,563. https://doi.org/10.1029/2019JA026839

Kakad, B., Gurram, P., Tripura Sundari, P. N. B., & Bhattacharyya, A. (2016). Structuring of intermediate scale equatorial spread F irregularities during intense geomagnetic storm of solar cycle 24. *Journal of Geophysical Research: Space Physics*, *121*, 7001–7012. https://doi.org/10.1002/2016JA022635

Kakad, B., Jeeva, K., Nair, K. U., & Bhattacharyya, A. (2007). Magnetic activity linked generation of nighttime equatorial spread F irregularities. *Journal of Geophysical Research*, *112*, A07311. https://doi.org/10.1029/2006JA012021

Kakad, B., Nayak, C., & Bhattacharyya, A. (2012a). Power spectral characteristics of ESF irregularities during magnetically quiet and disturbed days. *Journal of Atmospheric and Solar-Terrestrial Physics*, *81*, 41–49. https://doi.org/10.1016/j.jastp.2012.04.008

Kakad, B., Tiwari, D., & Pant, T. (2011). Study of disturbance dynamo effects at nighttime equatorial F region in Indian longitude. *Journal of Geophysical Research*, *116*, A12318. https://doi.org/10.1029/2011JA016626

Kakad, B., Tiwari, D., & Pant, T. (2012b). Study of post sunset vertical plasma drift at equatorial F-region using long-term (1990–2003) ionosonde measurements in Indian longitude. *Journal of Atmospheric and Solar-Terrestrial Physics*, *80*, 239–246. https://doi.org/10.1016/j.jastp.2012.02.004

Kane, R., & Echer, E. (2007). Phase shift (time) between storm-time maximum negative excursions of geomagnetic disturbance index dst and interplanetary bz. *Journal of Atmospheric and Solar-Terrestrial Physics*, *69*(9), 1009–1020. https://doi.org/10.1016/j.jastp.2007.03.008
Kelley, M. C., Baker, K., & Ulwick, J. (1979). Late time barium cloud striations and their possible relationship to equatorial spread F. *Journal of Geophysical Research*, *84*(A5), 1898–1904.
Kelley, M., Larsen, M., LaHoz, C., & McClure, J. (1981). Gravity wave initiation of equatorial spread F: A case study. *Journal of Geophysical Research*, *86*(A11), 9087–9100. https://doi.org/10.1029/JA086iA11p09087
Keskinen, M., Ossakow, S., Fejer, B. G., & Emmert, J. (2006). Evolution of equatorial ionospheric bubbles during a large auroral electrojet index increase in the recovery phase of a magnetic storm. *Journal of Geophysical Research*, *111*, A02303. https://doi.org/10.1029/2005JA011352
Kikuchi, T., Luhr, H., Schlegel, K., Tachihara, H., Shinohara, M., & Kitamura, T.-I. (2000). Penetration of auroral electric fields to the equator during a substorm. *Journal of Geophysical Research*, *105*(A10), 23,251–23,261. https://doi.org/10.1029/2000JA900016
Kil, H., Paxton, L. J., Lee, W. K., & Jee, G. (2019). Daytime evolution of equatorial plasma bubbles observed by the first Republic of China satellite. *Geophysical Research Letters*, *46*, 5021–5027. https://doi.org/10.1029/2019GL082903
Krall, J., Huba, J., & Fritts, D. (2013). On the seeding of equatorial spread F by gravity waves. *Geophysical Research Letters*, *40*, 661–664. https://doi.org/10.1002/grl.50144
Ledvina, B., Kintner, P., & de Paula, E. (2004). Understanding spaced-receiver zonal velocity estimation. *Journal of Geophysical Research*, *109*, A10306. https://doi.org/10.1029/2004JA010489
Li, G., Ning, B., Hu, L., Liu, L., Yue, X., Wan, W., et al. (2010). Longitudinal development of low-latitude ionospheric irregularities during the geomagnetic storms of July 2004. *Journal of Geophysical Research*, *115*, A04304. https://doi.org/10.1029/2009JA014830
Narayanan, V. L., Taori, A., Patra, A., Emperumal, K., & Gurubaran, S. (2012). On the importance of wave-like structures in the occurrence of equatorial plasma bubbles: A case study. *Journal of Geophysical Research*, *117*, A01306. https://doi.org/10.1029/2011JA017054
Navarro, L., Fejer, B., & Scherliess, L. (2019). Equatorial disturbance dynamo vertical plasma drifts over Jicamarca: Bi-monthly and solar cycle dependence. *Journal of Geophysical Research: Space Physics*, *124*, 4833–4841. https://doi.org/10.1029/2019JA026729
Niranjan, K., Brahmanandam, P., Rao, P. R., Uma, G., Prasad, D., & Rao, P. R. (2003). Post midnight spread-F occurrence over Waltair (17.7N, 83.3E) during low and ascending phases of solar activity. *Annales Geophysicae*, *21*(3), 745–750. https://doi.org/10.5194/angeo-21-745-2003
Nopper Jr, R., & Carovillano, R. (1978). Polar-equatorial coupling during magnetically active periods. *Geophysical Research Letters*, *5*(8), 699–702. https://doi.org/10.1029/GL005i008p00699
Ossakow, S. L. (1981). Spread-F theories: A review. *Journal of Atmospheric and Terrestrial Physics*, *43*(5–6), 437–452. https://doi.org/10.1016/0021-9169(81)90107-0, .
Patra, A., Rao, P., Anandan, V., & Jain, A. (1997). Radar observations of 2.8 m equatorial spread-F irregularities. *Journal of Atmospheric and Solar-Terrestrial Physics*, *59*(13), 1633–1641. https://doi.org/10.1016/S1364-6826(96)00162-9
Patra, A., Taori, A., Chaitanya, P., & Sripathi, S. (2013). Direct detection of wavelike spatial structure at the bottom of the F region and its role on the formation of equatorial plasma bubble. *Journal of Geophysical Research: Space Physics*, *118*, 1196–1202. https://doi.org/10.1002/jgra.50148
Retterer, J. (2010). Forecasting low-latitude radio scintillation with 3D ionospheric plume models: 1. Plume model. *Journal of Geophysical Research*, *115*, A03306. https://doi.org/10.1029/2008JA013839
Richmond, A., Peymirat, C., & Roble, R. (2003). Long-lasting disturbances in the equatorial ionospheric electric field simulated with a coupled magnetosphere-ionosphere-thermosphere model. *Journal of Geophysical Research*, *108*(A3), 1118. https://doi.org/10.1029/2002JA009758
Scherliess, L., & Fejer, B. G. (1997). Storm time dependence of equatorial disturbance dynamo zonal electric fields. *Journal of Geophysical Research*, *102*(A11), 24,037–24,046. https://doi.org/10.1029/97JA02165
Sekar, R., Suhasini, R., & Raghavarao, R. (1995). Evolution of plasma bubbles in the equatorial F region with different seeding conditions. *Geophysical Research Letters*, *22*(8), 885–888. https://doi.org/10.1029/95GL00813
Smith, J., & Heelis, R. A. (2017). Equatorial plasma bubbles: Variations of occurrence and spatial scale in local time, longitude, season, and solar activity. *Journal of Geophysical Research: Space Physics*, *122*, 5743–5755. https://doi.org/10.1002/2017JA024128
Smith, J. M., Rodrigues, F. S., Fejer, B. G., & Milla, M. A. (2016). Coherent and incoherent scatter radar study of the climatology and day-to-day variability of mean F region vertical drifts and equatorial spread F. *Journal of Geophysical Research: Space Physics*, *121*, 1466–1482. https://doi.org/10.1002/2015JA021934
Spiro, R., Wolf, R., & Fejer, B. G. (1988). Penetrating of high-latitude-electric-field effects to low latitudes during sundial 1984. *Annales Geophysicae*, *6*, 39–49.
Sultan, P. (1996). Linear theory and modeling of the Rayleigh-Taylor instability leading to the occurrence of equatorial spread F. *Journal of Geophysical Research*, *101*(A12), 26,875–26,891. https://doi.org/10.1029/96JA00682
Tiwari, D., Engavale, B., Bhattacharyya, A., Devasia, C., Pant, T., & Sridharan, R. (2006). Simultaneous radar and spaced receiver VHF scintillation observations of ESF irregularities. *Annales Geophysicae*, *24*(5), 1419–1427. https://doi.org/10.5194/angeo-24-1419-2006
Tsunoda, R. T. (1985). Control of the seasonal and longitudinal occurrence of equatorial scintillations by the longitudinal gradient in integrated E region Pedersen conductivity. *Journal of Geophysical Research*, *90*(A1), 447–456. https://doi.org/10.1029/JA090iA01p00447
Tsunoda, R. T. (2012). A simple model to relate ionogram signatures to large-scale wave structure. *Geophysical Research Letters*, *39*, L18107. https://doi.org/10.1029/2012GL053179
Valladares, C., Sheehan, R., Basu, S., Kuenzler, H., & Espinoza, J. (1996). The multi-instrumented studies of equatorial thermosphere aeronomy scintillation system: Climatology of zonal drifts. *Journal of Geophysical Research*, *101*(A12), 26,839–26,850. https://doi.org/10.1029/96JA00183
Yokoyama, T. (2017). A review on the numerical simulation of equatorial plasma bubbles toward scintillation evaluation and forecasting. *Progress in Earth and Planetary Science*, *4*(1), 37. https://doi.org/10.1186/s40645-017-0153-6
Yokoyama, T., Jin, H., Shinagawa, H., & Liu, H. (2019). Seeding of equatorial plasma bubbles by vertical neutral wind. *Geophysical Research Letters*, *46*, 7088–7095. https://doi.org/10.1029/2019GL083629
Yokoyama, T., Shinagawa, H., & Jin, H. (2014). Nonlinear growth, bifurcation, and pinching of equatorial plasma bubble simulated by three-dimensional high-resolution bubble model. *Journal of Geophysical Research: Space Physics*, *119*, 10,474–10,482. https://doi.org/10.1002/2014JA020708